

The Brewer–Dobson circulation inferred from ERA-Interim

William J. M. Seviour^{a,b}, Neal Butchart^a and Steven C. Hardiman^{a*}

^aHadley Centre, Met Office, Exeter, UK

^bCavendish Laboratory, Department of Physics, University of Cambridge, UK

*Correspondence to: S. C. Hardiman, Met Office, FitzRoy Road, Exeter EX1 3PB, UK.
E-mail: steven.hardiman@metoffice.gov.uk

The transformed Eulerian mean residual circulation is calculated from ERA-Interim for 1989–2009. Known as the Brewer–Dobson circulation, this measures the tropical upwelling of mass from troposphere to stratosphere, the mean meridional mass transport in the stratosphere and the downwelling of mass in the Extratropics. Major features of the Brewer–Dobson circulation, including the seasonal migration of the tropical upwelling toward the summer pole, are well represented. In the tropical lower stratosphere vertical velocities are less noisy than in other reanalyses, though significant tidal variations demonstrate the need for 6-hourly data. Throughout the year tropical lower stratospheric ascent rates are a minimum at the Equator and strongest in the Northern Hemisphere. In each hemisphere the maximum tropical ascent occurs during summer, whereas the strongest circulation and maximum in extratropical descent occur in the winter hemisphere. At 70 hPa the annual mean upwelling mass flux is $5.9 \times 10^9 \text{ kg s}^{-1}$, with the zonal drag from resolved waves and parametrized orographic gravity wave drag (OGWD) providing 70% and 4% of the driving, respectively. Hence it is concluded that the OGWD probably underestimates the momentum deposited above 70 hPa in addition to there being an absence of drag from non-orographic gravity waves. A statistically significant trend of -5% per decade in the upwelling mass flux is considered unreliable because it is inconsistent with the negative temperature trend, assuming a mainly adiabatic temperature response at this level (70 hPa) to the changes in upwelling. Copyright © 2011 British Crown copyright, the Met Office. Published by John Wiley & Sons Ltd.

Key Words: stratosphere; Brewer–Dobson circulation; ERA-Interim

Received 18 February 2011 ; Revised 11 October 2011; Accepted 11 October 2011; Published online in Wiley Online Library

Citation: Seviour WJM, Butchart N, Hardiman SC. 2011. The Brewer–Dobson circulation inferred from ERA-Interim. *Q. J. R. Meteorol. Soc.* DOI:10.1002/qj.966

1. Introduction

The Brewer–Dobson circulation describes the global-scale meridional circulation of the stratosphere, with upwelling in the Tropics and poleward and downward motion in the Extratropics. It has been of recent interest, with global models showing a consistent increase in the strength of the circulation associated with rising greenhouse gas concentrations (e.g. Butchart and Scaife, 2001; Butchart *et al.*, 2006, 2010; Garcia and Randel, 2008; Li *et al.*, 2008; McLandress and Shepherd, 2009). The Brewer–Dobson circulation

is very difficult to diagnose directly from meteorological observations and reanalysis data often provide the best tool for deriving its properties. The availability of ERA-Interim (Dee *et al.*, 2011)—the latest reanalysis dataset from the European Centre for Medium-Range Weather Forecasts (ECMWF)—provides a good opportunity to update our understanding of the basic features of the circulation.

There is currently a lack of consistency in how the strength of the Brewer–Dobson circulation (WMO, 2010) is characterized in terms of tropical upwelling. For instance, Randel *et al.* (2008) and Calvo and Garcia (2009) use fixed

latitude bands that do not include the Subtropics, while Butchart *et al.* (2006, 2010) and McLandress and Shepherd (2009) integrate the mass flux between the latitudes at which the upwelling changes sign (so-called ‘turnaround latitudes’; see section 4). The choice of vertical level also differs between these studies.

The aim of this study is to diagnose the major features of the Brewer–Dobson circulation and, in particular tropical upwelling from the newly available ERA-Interim reanalysis dataset. Tropical upwelling will be analysed directly using the residual vertical velocity (see section 2) and via the downward control principle (Haynes *et al.*, 1991), and long-term trends will be calculated. The effects of the different published approaches noted above for quantifying the strength of the Brewer–Dobson circulation in terms of upward tropical mass fluxes will be assessed and the implications for the analysed driving and calculated trends will be discussed.

2. Theoretical background

Since the Brewer–Dobson circulation describes Lagrangian-mean transport (in this paper we consider only the mean mass transport, not two-way mixing), it cannot be diagnosed directly from the Eulerian velocity. However, the transformed Eulerian mean (TEM) residual circulation (\bar{v}^* , \bar{w}^*) provides a useful proxy for the Lagrangian-mean motion under time-averaged conditions (e.g. Andrews and McIntyre, 1976; Dunkerton, 1978; Holton, 1990). In log(pressure) coordinates these are defined by

$$\bar{v}^* = \bar{v} - \frac{1}{\rho_0} \left(\frac{\rho_0 \overline{v'\theta'}}{\theta_z} \right)_z = -\frac{1}{\rho_0 \cos \phi} \frac{\partial \psi}{\partial z} \quad (1a)$$

and

$$\bar{w}^* = \bar{w} + \frac{1}{a \cos \phi} \left(\cos \phi \frac{\overline{v'\theta'}}{\theta_z} \right)_\phi = \frac{1}{a \rho_0 \cos \phi} \frac{\partial \psi}{\partial \phi}, \quad (1b)$$

where v and w are, respectively, the meridional and vertical components of the velocity, a is the Earth’s radius, ϕ is latitude, z is log(pressure) – height, $\rho_0 = \exp(-z/H)$, H is the density scale height taken as 6800 m and θ is potential temperature (hence, $w = -(H/p)(dp/dt)$, where p is the pressure). An overbar represents the zonal mean, and a

prime the deviation from this mean. Subscripts represent the partial derivative. The stream function for the residual flow is $\psi(\phi, z)$. Within the TEM formalism, the zonal momentum equation becomes

$$\bar{u}_t + \bar{v}^* \left(\frac{(\bar{u} \cos \phi)_\phi}{a \cos \phi} - f \right) + \bar{w}^* \bar{u}_z = DF + \bar{X} \equiv \bar{\mathcal{F}}, \quad (2)$$

where u is the zonal component of the velocity, f is the Coriolis parameter, X represents unresolved drag, and DF is a scaled version of the Eliassen–Palm (EP) flux divergence, i.e.

$$DF = \frac{\nabla \cdot \mathbf{F}}{\rho_0 a \cos \phi}, \quad (3)$$

where \mathbf{F} is the EP flux vector, with components

$$F^{(\phi)} = \rho_0 a \cos \phi \left(\bar{u}_z \frac{\overline{v'\theta'}}{\theta_z} - \overline{v'u'} \right) \quad (4a)$$

$$F^{(z)} = \rho_0 a \cos \phi \left\{ \left[f - \frac{(\bar{u} \cos \phi)_\phi}{a \cos \phi} \right] \frac{\overline{v'\theta'}}{\theta_z} - \overline{w'u'} \right\}. \quad (4b)$$

$\nabla \cdot \mathbf{F}$ represents forcing due to resolved wave breaking.

For a realistic and steady (i.e. $\bar{u}_t = 0$) zonal mean zonal wind distribution $\bar{u}(\phi, z)$, $\bar{v}^* = \bar{w}^* = 0$ is a solution of Eq. (2) in the absence of wave driving (i.e. if $\bar{X} = 0$ and $DF = 0$). The introduction of non-zero wave forcing terms (\bar{X} and/or DF) will then generally result in the TEM residual circulation also becoming non-zero to maintain the steady conditions. Hence under this approximation the Brewer–Dobson circulation can be considered as a wave-driven circulation. Moreover, for the steady conditions, the downward control principle of Haynes *et al.* (1991) allows the stream function of the residual circulation, $\psi(\phi, z)$, to be expressed in terms of a vertical integral of the total forcing term from Eq. (2):

$$\psi(\phi, z) = \int_z^\infty \left\{ \frac{\rho_0 a \bar{\mathcal{F}} \cos^2 \phi}{\bar{m}_\phi} \right\}_{\phi=\phi(z')} dz', \quad (5)$$

where $\bar{m} = a \cos \phi (\bar{u} + a\Omega \cos \phi)$ is the angular momentum per unit mass and Ω is the angular velocity of the Earth’s rotation. The integration is along a line of constant angular

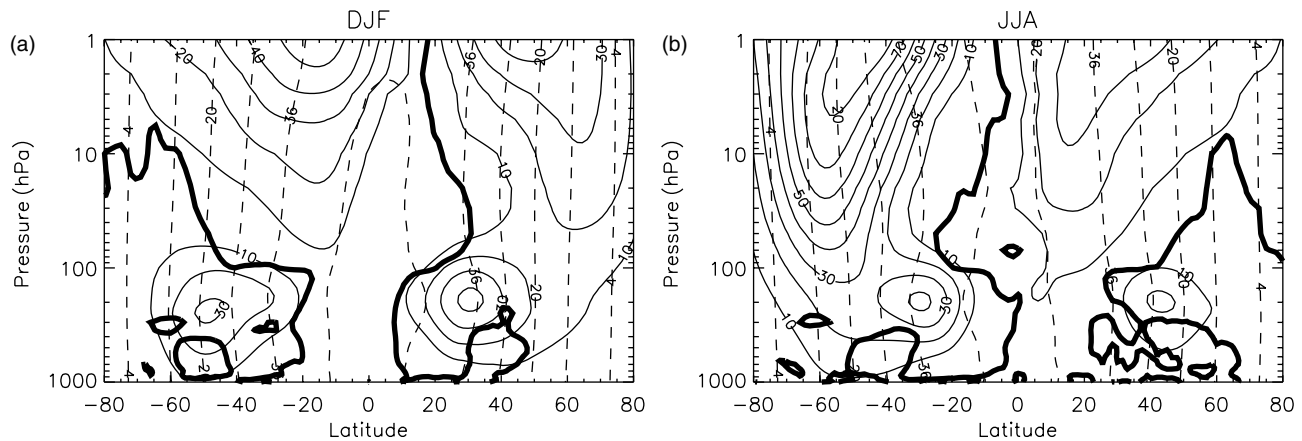


Figure 1. December–January–February (DJF) and June–July–August (JJA) climatological averages (1989–2009) of zonal mean zonal wind (solid line, in units of m s⁻¹) and zonal mean absolute angular momentum per unit mass (dashed line, in units of 6.4 × 10⁷ m² s⁻¹) from ERA-Interim. The bold solid line is a contour of $\bar{w}^* = 0$, indicating the extent of tropical upwelling, or the ‘tropical pipe’.

momentum, which is approximated as vertical, but this breaks down near the Equator (cf. dashed contours in Figure 1). By splitting \overline{F} into its resolved (DF) and unresolved (\overline{X}) components in Eq. (5) the contribution from each of these components in driving the upwelling can be quantified.

3. Assimilation models and data

3.1. Models

The ECMWF Interim Reanalysis (ERA-Interim; Dee *et al.*, 2011) data incorporate observations from *in situ* measurements, balloons, radiosondes, dropsondes, aircraft and satellites (Simmons *et al.*, 2007). The assimilation uses the ECMWF Integrated Forecast System (IFS) model, run at a horizontal resolution of T255, with 60 vertical levels and including physical parametrization schemes for radiative transfer, turbulent mixing, sub-grid-scale orographic drag, moist convection, clouds and surface/soil processes (IFS Documentation, 2007). A Rayleigh friction and diffusion are also included in the model. ERA-Interim is similar to the ERA-40 Reanalysis (Uppala *et al.*, 2005) but uses ECMWF's operational four-dimensional variational data assimilation system (4D-Var) as opposed to the 3D-Var system used in ERA-40, and has improved humidity analysis, model physics, data quality control, bias handling and other improvements as noted in Simmons *et al.* (2007). Although ozone is actively assimilated in ERA-Interim (Dragani, 2010), the sensitivity of mass and wind variables to ozone data is switched off, and only an ozone climatology is used in the radiation scheme. Therefore the meteorological variables are not affected by the assimilated ozone. Greenhouse gases are set to observed 1990 values plus a linear trend (as specified in Houghton *et al.*, 1995). In particular, carbon dioxide is assumed to be well mixed with a concentration of 353 ppmv + 1.5 ppmv per year.

The UK Met Office (UKMO) stratospheric analysis (Swinbank and O'Neill, 1994) are also used in this study, to support the ERA-Interim results. The assimilation uses the Met Office Unified Model (Davies *et al.*, 2005). There was a major change in the dynamical core of the assimilation model in 2003 and therefore only data for 2004–2009 are used in this study. Data are obtained at a resolution of 3.75° longitude \times 2.5° latitude as daily instantaneous fields (at 1200 UTC), though the vertical velocity is averaged over all assimilation time steps from 0900 UTC to 1500 UTC.

3.2. Data

The ERA-Interim data are available over the period 1989–2009, and obtained here on 37 pressure levels with a 1.5° horizontal resolution. The uppermost pressure level obtained is at 1 hPa with vertical resolution approximately 1 km throughout the stratosphere. These data have a good representation of the stratosphere, as can be seen by the zonal mean zonal wind shown in Figure 1. The polar jets are represented clearly, with stratospheric flow largely eastward in the winter hemisphere and westward in the summer hemisphere.

Data are obtained at 6-hourly time intervals at the four main synoptic times 0000, 0600, 1200 and 1800 UTC. Figure 2 illustrates the importance of using data with at least this temporal resolution, showing the residual mean vertical velocity, \overline{w}^* , at 70 hPa for both 6-hourly and daily sampling rates. There is a clear anti-phase relationship between the daily data sampled at 0600 UTC and 1200 UTC, suggestive of a strong variation in upwelling with a 12-hour period. A similar relationship exists between data sampled at 0000 UTC and 1800 UTC. The greatest difference between 6-hourly and daily sampled data occurs in the Tropics and it is clear that a minimum of a 6-hourly sampling rate is necessary for calculating properties of tropical upwelling. Further, work comparing the residual mean vertical velocity in the Met Office Unified Model calculated every model time step (20 minutes), 6-hourly and daily shows that, in fact,

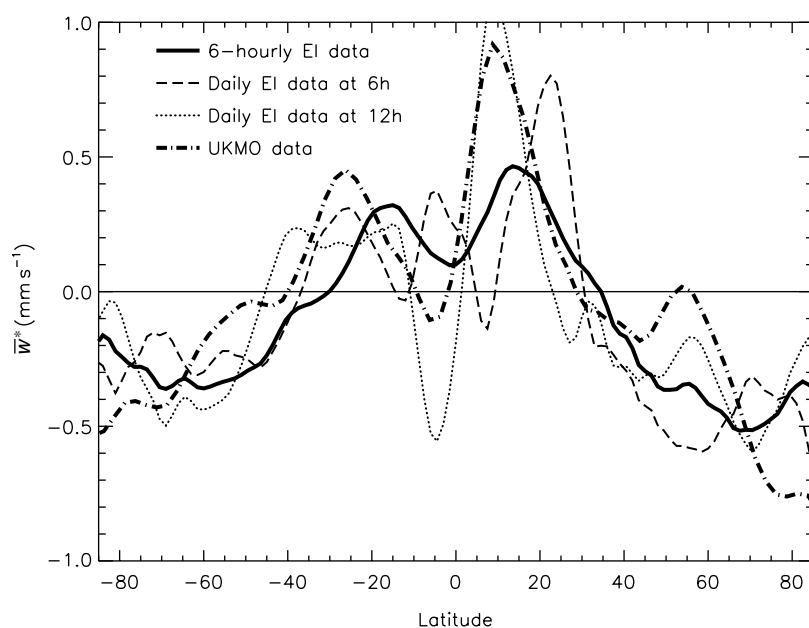


Figure 2. Annual mean \overline{w}^* at 70 hPa for 6-hourly sampling rates (at 0000 UTC, 0600 UTC, 1200 UTC, and 1800 UTC) and daily sampling rates at 0600 UTC and 1200 UTC from ERA-Interim for 1989–2009. Annual mean \overline{w}^* at 68 hPa from the UKMO analysis (2004–2009) is also shown; this is available daily, averaged between 0900 UTC and 1500 UTC.

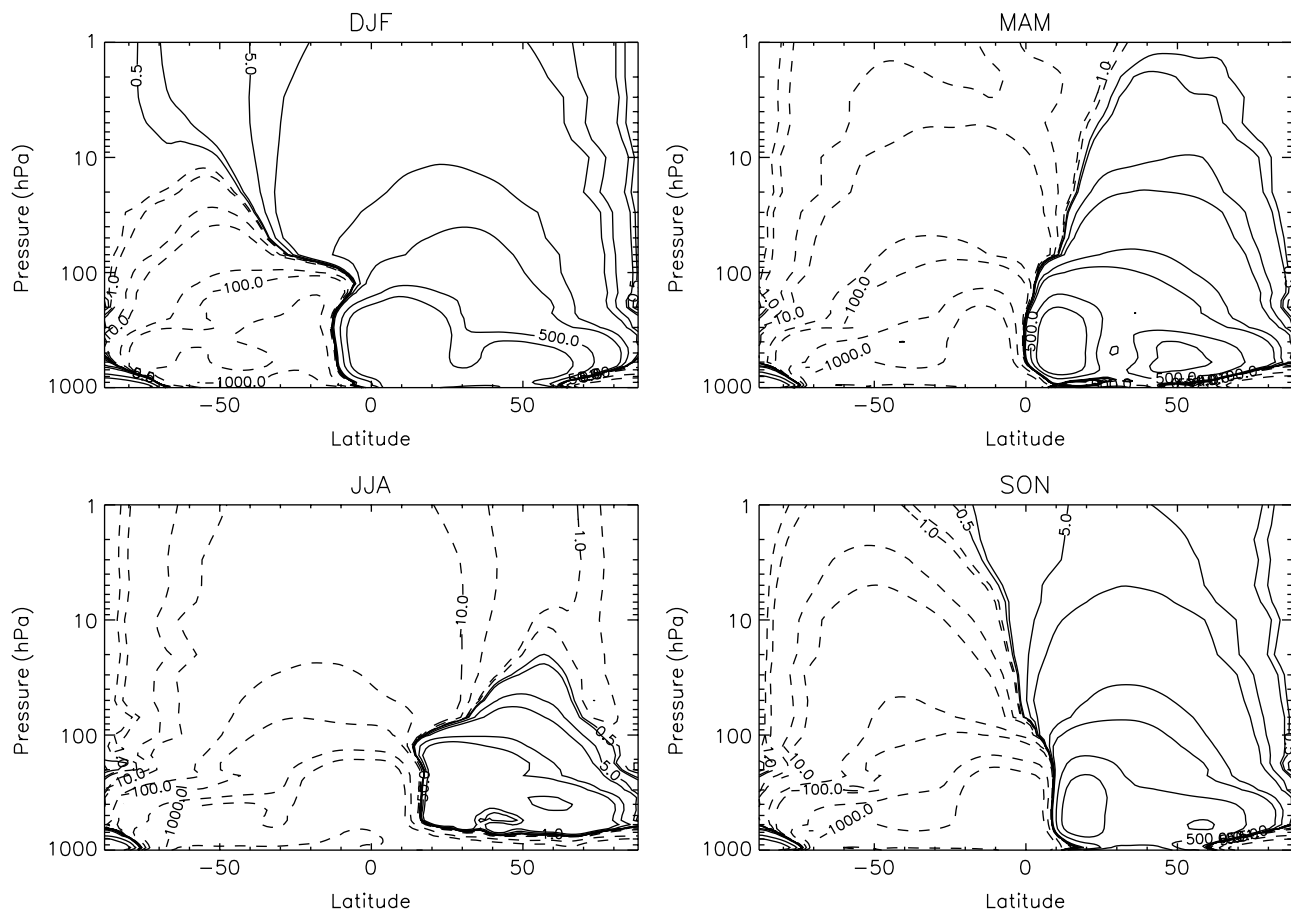


Figure 3. Seasonal mean TEM stream function from ERA-Interim for 1989–2009. Contours have units of $\text{kg m}^{-1} \text{s}^{-1}$ and are spaced logarithmically. Dashed contours represent negative values.

6-hourly data are sufficient (not just necessary) to accurately diagnose \bar{w}^* in the lower stratosphere (not shown).

Figure 2 also shows the annual mean \bar{w}^* at 68 hPa determined from the UKMO analysis. The UKMO data show larger upwelling in the Tropics than 6-hourly ERA-Interim, and the turnaround latitudes (the latitudes at which \bar{w}^* changes sign) are shifted further south. However, there is generally good agreement in the profile and magnitude of upwelling between the two datasets.

4. Brewer–Dobson circulation

4.1. The transformed Eulerian-mean circulation

The climatology of the seasonal mean TEM stream function defined in Eq. (1) is shown in Figure 3 for the ERA-Interim data from 1989 to 2009. The stream function was calculated by assuming \bar{w}^* was zero at 90°N and 90°S and integrating Eq. (1b) from north to south and south to north, respectively, then taking the average. A very similar result (not shown) was obtained by integrating Eq. (1a) downward from the top level assuming \bar{v}^* was zero above that level. All the major features of the Brewer–Dobson circulation are clearly seen in the figure; upwelling in the Tropics and poleward–downward flow in the Extratropics. There is a prominent annual cycle, with the upwelling displaced from the Equator toward the summer hemisphere and the strongest downwelling in the winter hemisphere. The shift of the upwelling to the summer hemisphere becomes more

pronounced with altitude. In the troposphere the Hadley cell is clearly visible in the stream function.

The annual cycle of the Brewer–Dobson circulation is again seen in the latitude–month variation of \bar{w}^* at 70 hPa and 100 hPa (Figure 4(a) and (c), respectively) with the region of tropical upwelling, or ‘tropical pipe’, oscillating between summer hemispheres by approximately 20° in latitude at 70 hPa. Interestingly, this seasonal migration of the edge of the tropical pipe toward the pole in spring and then back toward the Equator in autumn is roughly the same as that seen for the latitude of the zero zonal mean zonal wind line in the lower stratosphere (not shown). The ERA-Interim residual vertical velocities in Figure 4(a) and (c) are broadly similar to those obtained from the 6 years of UKMO analysis data for 2004–2009 (Figure 4(b) and (d)). Compared to \bar{w}^* derived from ERA-40 (cf. Randel *et al.*, 2008, their Figure 1) the annual cycle in the tropical upwelling is more smoothly represented in ERA-Interim, most likely due to the use of 4D-Var data assimilation as opposed to the 3D-Var assimilation used in the production of ERA-40 (Simmons *et al.*, 2007). Using mass-weighted isentropic diagnostics, Iwasaki *et al.* (2009) also found that ERA-Interim, along with the JRA-25 reanalysis (Onogi *et al.*, 2007), had less noisy zonal mean vertical velocities at 50 hPa compared to other reanalysis datasets.

The vertical structure of the tropical pipe averaged for December to February (DJF) and June to August (JJA) further indicates that the displacement of the pipe toward the summer hemisphere increases with altitude (Figure 1, thick bold lines). At about 100 hPa there is a rapid increase

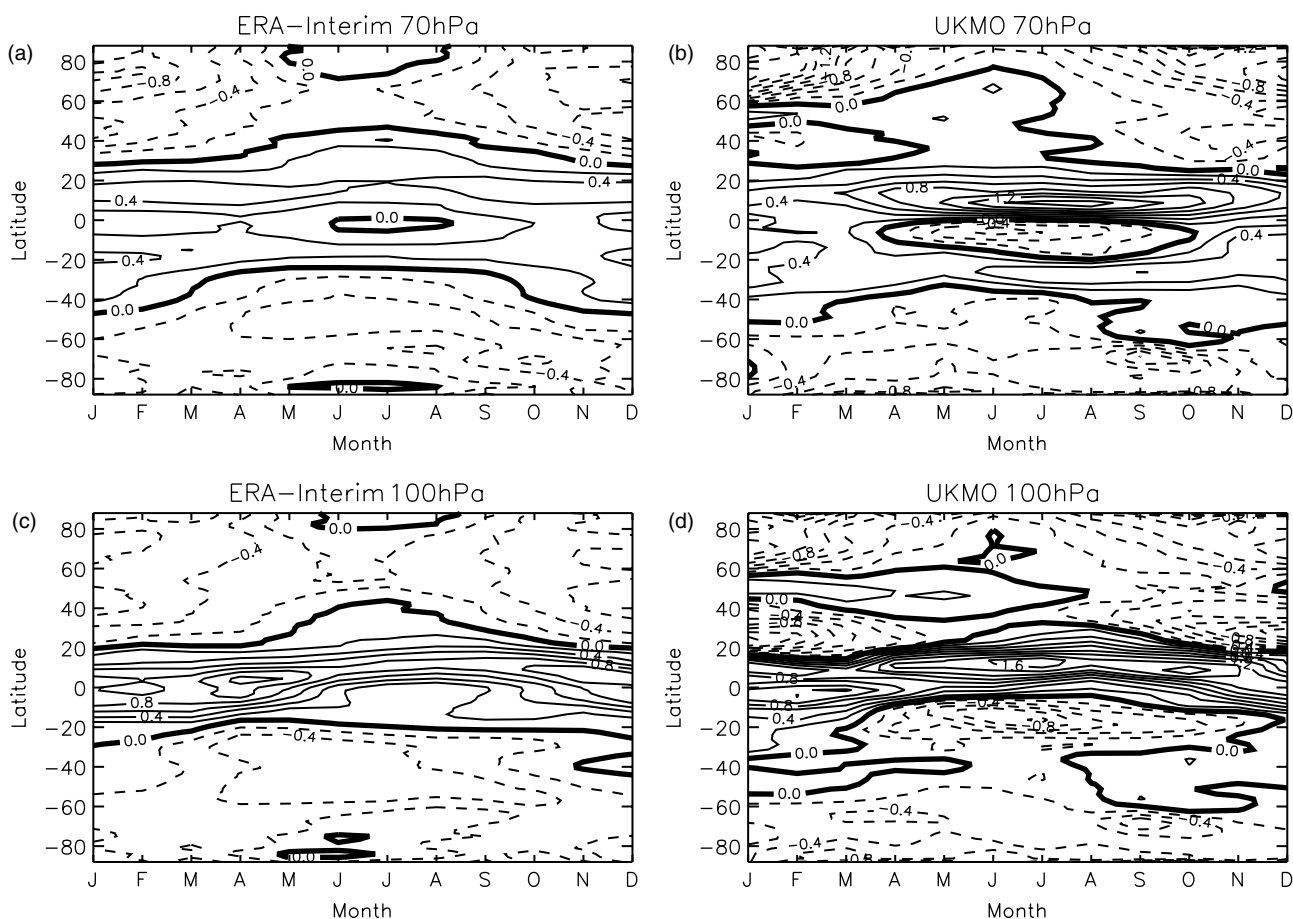


Figure 4. Monthly and latitudinal variations of monthly mean \bar{w}^* at (a) and (b) 70 hPa, and (c) and (d) 100 hPa for both (a) and (c) ERA-Interim data for 1989–2009, and (b) and (d) UKMO data for 2004–2009. Contours are in units of mm s^{-1} , with the zero contour in bold. Dashed contours represent negative values.

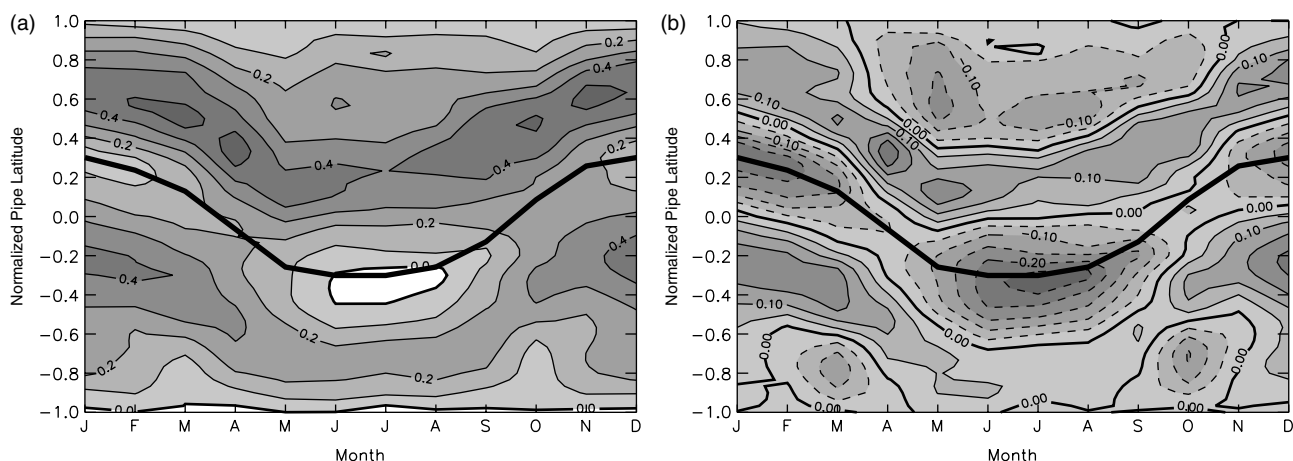


Figure 5. For ERA-Interim for 1989–2009. (a) Monthly average \bar{w}^* (70 hPa) within the tropical pipe, transformed to normalized pipe latitude such that latitude 0 always represents the centre of the pipe. The bold line represents the Equator in the transformed coordinates. Contours are in units of mm s^{-1} . (b) As (a) but with annual mean removed at each normalized pipe latitude.

with altitude in the width of the pipe and above 10 hPa the region of upwelling extends all the way to the summer pole (see Figure 1). These results are similar to those of Rosenlof (1995) and Eluszkiewicz *et al.* (1996), who derived \bar{w}^* from diabatic heating rates.

An advantage of the smoother representation of the tropical upwelling in ERA-Interim compared to ERA-40 is that it allows the distribution of the upwelling within the pipe to be examined in more detail than with the earlier

reanalysis or analysis datasets. To remove the effects of the seasonal movement of the pipe toward and away from the summer hemisphere, and the seasonal changes in pipe width, the monthly and latitudinal variations in the strength of the upwelling are shown in Figure 5(a) using a transformed meridional coordinate that runs from -1 to $+1$ at the southern and northern edges of the pipe, respectively (see figure caption for details). The location of the Equator in these coordinates is indicated by the thick bold line. This is

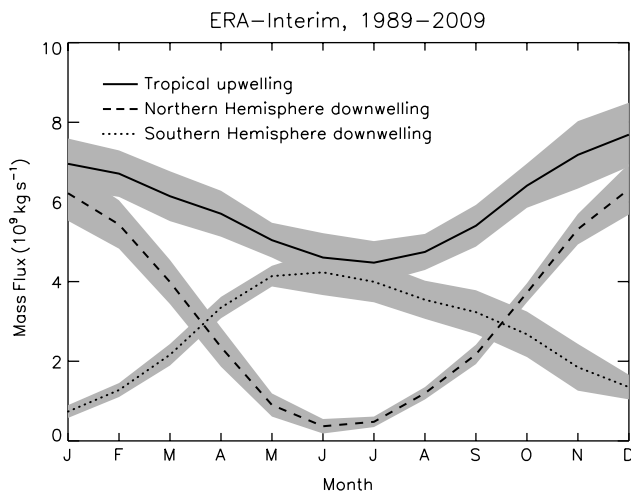


Figure 6. Climatological mass flux across 70 hPa from ERA-Interim (1989–2009). Tropical upwelling is calculated between turnaround latitudes, and downwelling is calculated between the turnaround latitude and the respective pole. The shading denotes the interannual standard deviation.

also the location of the weakest upwelling within the pipe and, from June to August, \bar{w}^* at the Equator is approximately zero, confirming the local equatorial minimum in \bar{w}^* noted by Butchart *et al.* (2006).

Although the movement of the Equator in the transformed coordinates in Figure 5(a) is consistent with the well-known displacement of the tropical pipe toward the summer hemisphere, (e.g. Holton, 1990) the figure also indicates that throughout the year the fastest ascent rates (as indicated by the largest upward velocities) are found in the northern half of the pipe and, indeed, in the Northern Hemisphere. Near the centre of the pipe, the annual cycle in ascent rates has opposite phases in the northern and southern halves of the pipe, with ascent during the extended summer period in each hemisphere (see Figure 5(b), which shows tropical upwelling with the annual mean value removed at each normalized pipe latitude). This contrasts to the extratropical downwelling, which is a maximum in each hemisphere during winter (see below and in particular Figure 6), demonstrating cross-equatorial transport in the stratosphere.

On moving toward the edges of the pipe the seasonal variations in the upwelling become more semi-annual than annual, with weaker (stronger) ascent during the equinox (solstice) seasons in both hemispheres (Figure 5(b)). This is most likely a consequence of a similar semi-annual variation in the quasi-horizontal areal cross-section of the pipe such that the pipe size is a minimum during the two equinox seasons (not shown). In turn, this arises because the duration in each hemisphere of the poleward displacement of the turnaround latitude during summer is less than 6 months and hence there are months when neither turnaround latitude is displaced poleward (e.g. see Figure 4(a)). However, for most months the area of tropical ascent is slightly larger than the area of extratropical descent and when averaged over the whole year is 53.3% of the global surface area.

4.2. Mass flux

The upward tropical mass flux within the pipe is the mass per unit time flowing between turnaround latitudes ϕ_+ and ϕ_- at which \bar{w}^* changes sign north and south of the Equator,

respectively, i.e.

$$\text{upward tropical mass flux} = 2\pi \int_{\phi_-}^{\phi_+} \bar{w}^* \rho_0 a^2 \cos \phi \, d\phi. \quad (6)$$

This flux, calculated at 70 hPa, is shown in Figure 6. Also shown in the figure are the extratropical downward mass fluxes in each hemisphere, calculated by integrating from the relevant pole to the turnaround latitude. As expected from mass conservation, the sum of the extratropical downward mass fluxes equals the tropical upwelling mass flux.

In each hemisphere there is a strong annual cycle, with the hemispheric downwelling reaching a maximum during winter, then falling to almost zero during the summer (Figure 6). Again there is a 6-month phase difference between the two hemispheres and, because the winter maximum is greatest in the Northern Hemisphere, the annual cycle in the tropical upwelling is in phase with that of the Northern Hemisphere downwelling. For all three curves in the figure the interannual variability is much smaller than the amplitude of the annual cycle. Comparing Figures 5 and 6 also suggests that, in general, the wintertime extratropical downwelling is balanced by tropical upwelling that occurs mainly in the opposite hemisphere, confirming that the pumping action of the wave driving reaches into the opposite hemisphere, as has been noted for large-scale transient events (e.g. Dunkerton *et al.*, 1981; Randel, 1993; Holton *et al.*, 1995; Plumb and Eluszkiewicz, 1999).

4.3. Wave drag and downward control

The seasonal mean scaled EP flux divergence (DF) and forcing due to parametrized processes (\bar{X}) are plotted in Figure 7 for the two solstice seasons. The greatest planetary wave breaking is seen to occur in the winter hemisphere, of which the Northern Hemisphere has the largest magnitude. Planetary (resolved) wave breaking also extends further poleward in the Northern Hemisphere (DJF) than in the Southern Hemisphere (JJA) (Figure 7(a)).

The parametrized forcing \bar{X} is largely westward in Figure 7(b). This is due to the absence of parametrized *non-orographic* gravity wave drag in the IFS model used for ERA-Interim (IFS Documentation, 2007) such that \bar{X} represents only orographic gravity wave drag, at least in the stratosphere. Parametrizations of non-orographic gravity waves can, in general, produce weak eastward drag in the high-latitude winter lower stratosphere of about 0.5 ms^{-1} per day (e.g. see Figure 3 of Scaife *et al.*, 2002). This is typically weaker than the westward drag produced at higher altitudes by such schemes but is comparable in magnitude to the westward drag from the resolved waves (DF) and parametrized orographic waves (\bar{X}) in the lower stratosphere in Figure 7.

Figure 8 compares the DJF and JJA mean stream function at 70 hPa calculated directly from \bar{w}^* (see Eq. (1)) with that derived from the scaled EP flux divergence DF and parametrized forcing \bar{X} assuming downward control (see Eq. (5) and figure caption for details). The stream function calculated from DF (i.e. the resolved wave forcing) agrees well with that obtained directly from \bar{w}^* apart from between about 20° and 50° , particularly in the winter hemisphere. Because this difference is only partially accounted for ($\sim 35\%$

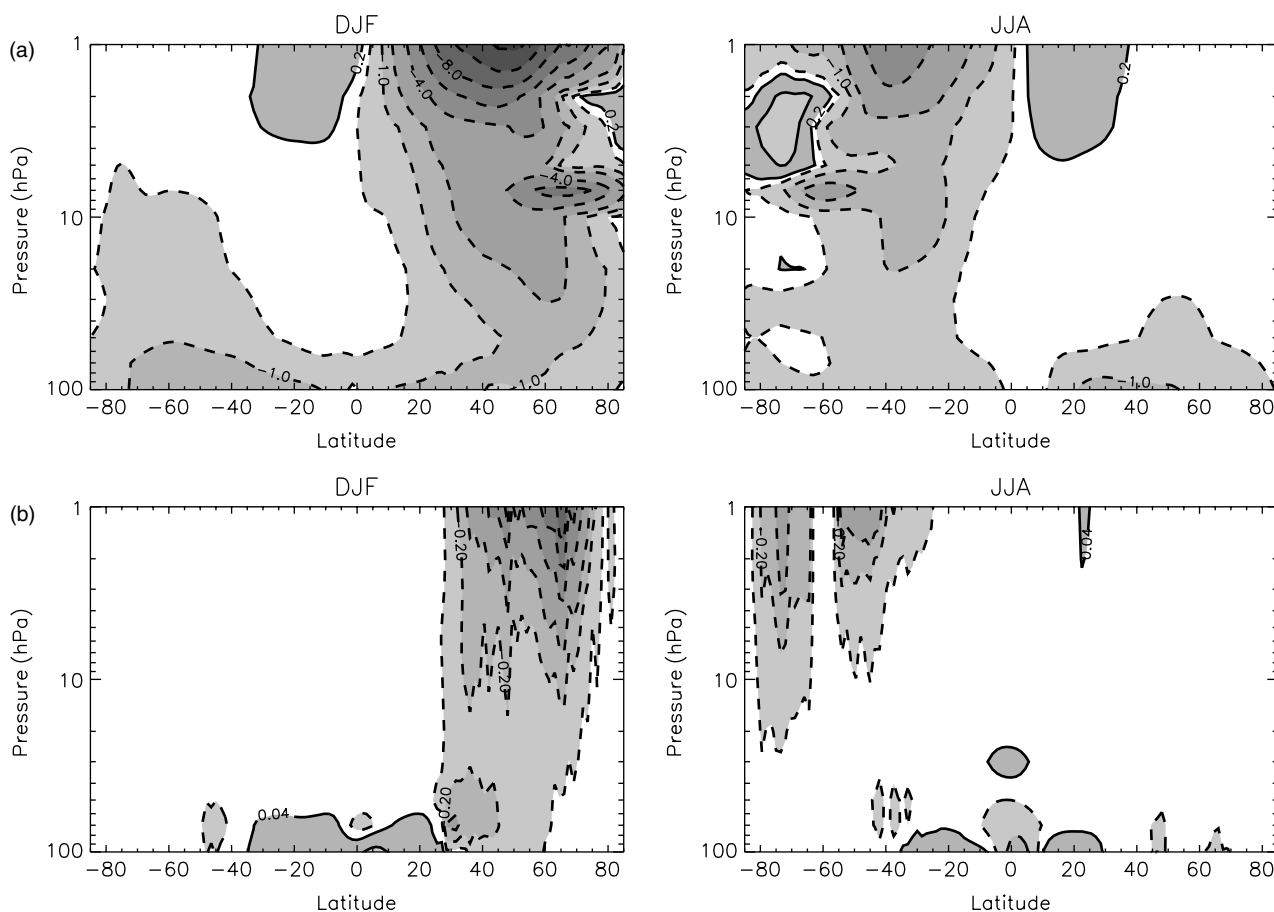


Figure 7. Seasonal average of (a) resolved wave drag (DF) and (b) parametrized wave drag (\bar{X}) in the stratosphere from ERA-Interim (1989–2009). Contours have units of m s^{-1} per day.

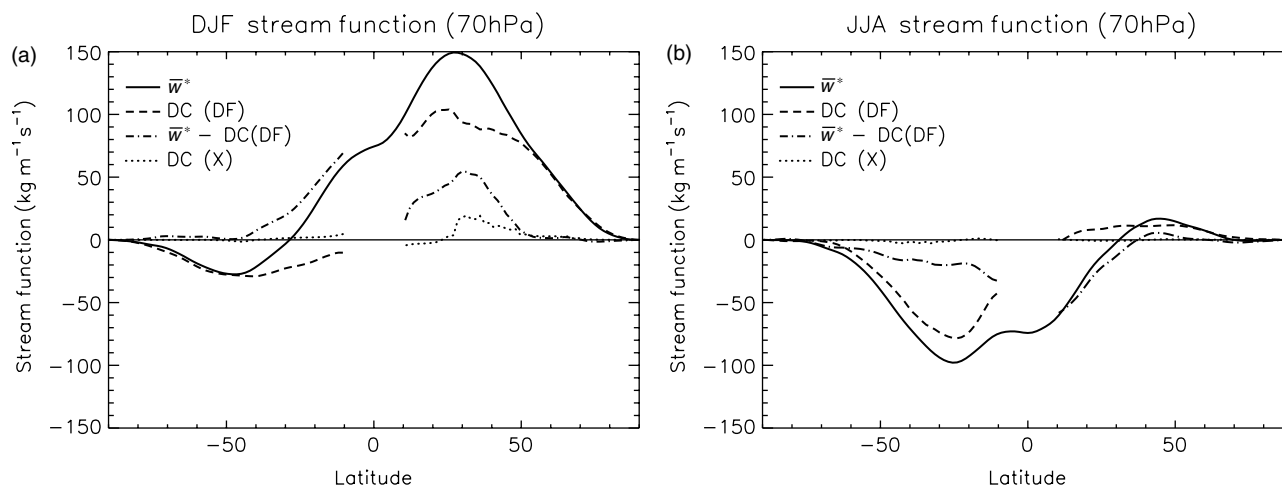


Figure 8. For ERA-Interim for 1989–2009, mass stream function at 70 hPa for (a) DJF and (b) JJA calculated from \bar{w}^* , resolved waves (DF) and parametrized processes (\bar{X}) using downward control (DC), and the difference between stream functions calculated from \bar{w}^* and DF.

between $\sim 30^\circ\text{N}$ and 50°N in DJF) by the contribution from the parametrized drag \bar{X} (dotted line in Figure 8) this suggests that in the IFS model the orographic gravity wave drag parametrization (i.e. \bar{X}) is perhaps underestimating the momentum deposited by these waves above 70 hPa by up to a factor of three, at least in this latitude band in DJF. On the other hand, if the parametrized waves already break (i.e. saturate) below 70 hPa it would be difficult to significantly increase the upward flux of momentum above that level as only the unsaturated part of the momentum flux

is allowed to propagate upward. Therefore, other processes such as parametrized non-orographic gravity wave drag almost certainly play a role, particularly toward the Tropics, where sub-grid-scale gravity waves from convective sources are likely to be important (Chun *et al.*, 2004). For the DJF (JJA) results shown in Figure 8, 70% (75%) of the tropical upwelling (or more strictly the corresponding extratropical downwelling) is due to resolved waves (i.e. DF) and 8% (1%) due to parametrized forcing (i.e. \bar{X}), with the remainder due to missing processes such as non-orographic gravity wave

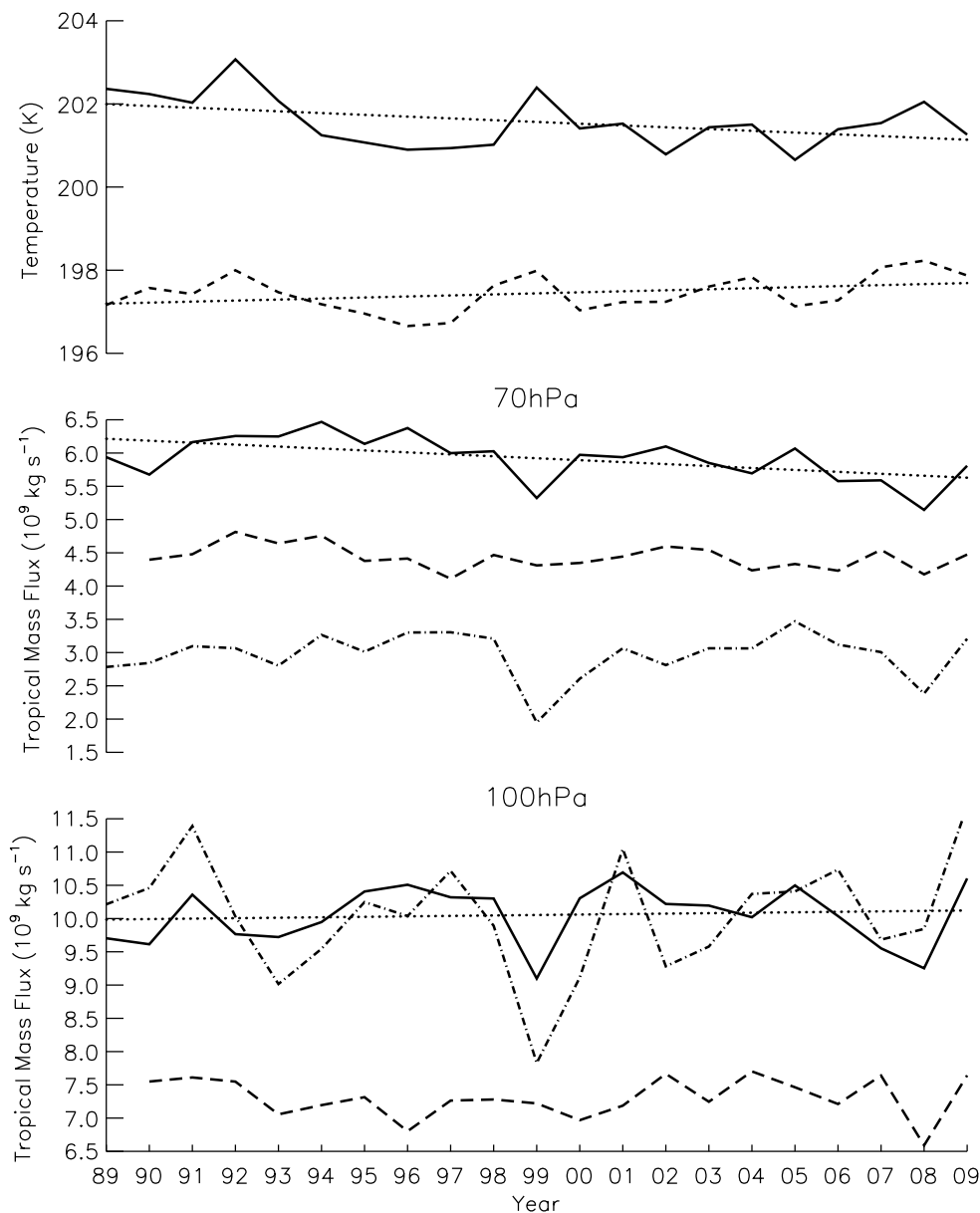


Figure 9. Time series for ERA-Interim of annual mean (top) temperature averaged between turnaround latitudes at 70 hPa (solid line) and 100 hPa (dashed line), and (middle and bottom) tropical upwelling at 70 hPa and 100 hPa, calculated between turnaround latitudes (solid line), between fixed latitudes 15°S–15°N (dot-dashed line) and via downward control between turnaround latitudes (dashed line).

drag. When averaged over the whole year (not shown) the corresponding percentages are 70% for the resolved waves (DF) and 4% for the parametrized forcing (\bar{X}). Rayleigh friction is included in the model above 10 hPa, but its contribution to tropical upwelling is found to be just 0.4% (not shown). It should be noted that data are only available up to 1 hPa; thus the influence of the mesosphere is not included in these downward control calculations.

These results show that the state-of-the-art chemistry–climate models analysed in Butchart *et al.* (2011) represent well the contribution of resolved wave forcing to driving the annual mean tropical upwelling at 70 hPa. Butchart *et al.* (2011) found the average contribution across the chemistry–climate models to be 70.7% from resolved waves, 21.1% from orographic gravity wave drag (parametrized in ERA-Interim) and 7.1% from non-orographic gravity wave drag (not included in ERA-Interim).

Another notable feature of the DJF stream function calculated from the EP flux divergence (Figure 8(a),

dashed curve) is its relatively flat profile near the northern turnaround latitude (i.e. the latitudes of the local maxima of the solid curve where $\bar{w}^* = \frac{1}{a\rho_0 \cos \phi} \frac{\partial \psi}{\partial \phi} = 0$). The flat dashed curve implies that \bar{w}^* resulting from DF is zero either side of the turnaround latitudes and consequently the extratropical downwelling driven by the EP flux divergence is not particularly sensitive to the location of the turnaround latitudes, in contrast to the findings of McLandress and Shepherd (2009). As a corollary to this, most of the latitudinal variability of \bar{w}^* near the edge of the tropical pipe is determined by the sub-grid-scale forcing \bar{X} and other missing unresolved processes.

4.4. Time series: long-term trends

Figure 9 shows, for ERA-Interim, the time series of the annual mean tropical temperatures and upwelling at both 70 hPa and 100 hPa, and averaged between the turnaround

Table I. Trends plus standard error in tropical upwelling series shown in Figure 9. Values are expressed as a percentage of the 20-year average, along with the standard error.

Tropical upwelling trends (% per decade)	
Turnaround latitudes, 70 hPa	-5 ± 2
Fixed 15°S–15°N, 70 hPa	0 ± 5
Turnaround latitudes, 100 hPa	1 ± 2
Fixed 15°S–15°N, 100 hPa	1 ± 4

latitudes. The upwelling results are also shown averaged between 15°S and 15°N (as in Randel *et al.*, 2008). At 70 hPa the annual mean upwelling mass flux calculated between the turnaround latitudes and averaged over the 20 years is $5.9 \times 10^9 \text{ kg s}^{-1}$. This is in good agreement with the $6.2 \times 10^9 \text{ kg s}^{-1}$ calculated between turnaround latitudes at 68 hPa for the UKMO stratospheric analyses for 2004–2009 and also with the multi-model mean value of $5.9 \times 10^9 \text{ kg s}^{-1}$ calculated by Butchart *et al.* (2011) for a range of climate-chemistry models, again at 70 hPa.

For the four upwelling time series shown in Figure 9 that are calculated directly from \bar{w}^* , the corresponding long-term trends are listed in Table I as a percentage of the 20-year mean. The only significant non-zero trend (that for which the size of the uncertainty is not larger than the size of the trend) is that calculated between the turnaround latitudes for the upwelling at 70 hPa, which is decreasing. Trends calculated for the other three time series are not statistically significantly different from zero at the 95% confidence level. Therefore, for the 20 years of ERA-Interim data, trends in the Brewer–Dobson circulation inferred from tropical upwelling are dependent on both the precise level at which the upwelling is calculated and also the range of upwelling latitudes included. Nonetheless, none of the four time series support the statistically significant increase in upwelling that has been predicted by models as a consequence of the increasing amounts of CO₂ in the atmosphere (e.g. Butchart *et al.*, 2010). Based on expected changes in adiabatic heating the statistically significant negative temperature trend at 70 hPa in Figure 9 is also not consistent with the long-term decrease in upwelling at 70 hPa though, interestingly, the anti-correlation (correlation coefficient of -0.65 for the detrended time series) of the interannual variability in the two time series confirms an adiabatic temperature response to the upwelling on the shorter time-scale. Further, as discussed in section 3.1, the effects of ozone trends are not included in ERA-Interim, which may in part explain this inconsistency. Thus it is suggested that although the climatology of \bar{w}^* is considered robust, the trends in \bar{w}^* should be considered unreliable.

Figure 9 also includes mass flux calculated using downward control (Eq. (5)). As already noted in section 4.3, the downward control values are consistently less than those found directly from upwelling. Other than the apparent direct intrusion from troposphere to stratosphere of reduced upwelling in 1999, downward control captures interannual variability well and the correlation coefficient with the directly calculated mass flux is 0.7 at 70 hPa. The slight downward trend in upwelling at 70 hPa is also captured. As already mentioned, in 1999 a decrease is seen in upwelling, with a corresponding increase in temperature, that is not captured by downward control. That the anomalies in

temperature and upwelling are of opposite sign is consistent with a change in upwelling driving a change in temperature here. That the signal is not captured by downward control suggests the forcing is directly from below, in this case through an upward extension of the radiative–convective heating of the troposphere.

5. Conclusions

The major features of the Brewer–Dobson circulation, including tropical upwelling into the stratosphere and poleward and downward flow in the Extratropics, have been found to be reproduced in ERA-Interim. The annual cycle, with the greatest upwelling in the Northern Hemisphere winter and movement of the ‘tropical pipe’ between summer hemispheres, is also well represented.

Considering the effect of sampling frequency on calculating the transformed Eulerian-mean residual vertical velocities, a strong tidal variation was found which is greatest in the Tropics. Tidal fluctuations are a known feature of other ECMWF-produced analyses in the lower stratosphere and have been shown to be consistent with tidal theory (Hsu and Hoskins, 1989). Consequently, a minimum 6-hourly sampling was found necessary for diagnosing the climatology of the Brewer–Dobson circulation. Further analyses of model results suggests the 6-hourly sampling is also sufficient to provide an accurate representation of the diurnally averaged circulation.

The much smoother representation of the residual vertical velocity in ERA-Interim compared to other reanalysis datasets (e.g. ERA-40; see also Iwasaki *et al.*, 2009) allowed the spatial structure of the upwelling within the tropical pipe to be diagnosed in more detail than had been previously possible. In the lower stratosphere (70 hPa) it was found that ascent rates within the pipe were a minimum (zero from June to August) at the Equator and, throughout the year, the fastest ascent always occurred in the Northern Hemisphere. In both hemispheres the ascent was generally stronger during summer than winter, in contrast to the extratropical descent, which is a maximum during winter in each hemisphere. Seasonal variations in the areal size (width) of the tropical pipe were more semi-annual than annual, with the minimum size occurring in the two equinox seasons. This was because the winter regime in which the edge of the tropical pipe is displaced equatorward lasts longer than the summer regime.

In the lower stratosphere (70 hPa) the annual mean upward tropical mass flux in ERA-Interim was $5.9 \times 10^9 \text{ kg s}^{-1}$. This is a robust figure, consistent with mass fluxes obtained from other analyses and climate-chemistry model simulations. Seventy per cent of the annual mean upwelling was driven by the resolved waves, with the unresolved drag (essentially parametrised orographic gravity wave drag) in the ERA-Interim model providing only 4% of the driving. It was argued that this imbalance between the downward control estimates and the actual upwelling mass flux resulted, first, from the parametrized orographic gravity wave drag underestimating the momentum deposited above 70 hPa, particularly in the northern Subtropics and, secondly, the absence of sub-grid-scale drag from non-orographic gravity waves (e.g. waves with convective sources).

Over the 20 years 1989–2009 it was found that trends in the upwelling mass flux depended on both the level chosen (100 or 70 hPa) and whether or not the flux in the whole

tropical pipe or just an equatorial latitude band (i.e. 15°S–15°N) was considered. Only the trend at 70 hPa for the flux in the whole pipe was statistically significantly different from zero. As this includes all the upward mass flux, and there is unlikely to be any two-way mass exchange at this level, unlike 100 hPa, this is arguably the most useful zeroth-order measure of the overall strength of the Brewer–Dobson circulation. For the ERA-Interim it was estimated that this measure of the upwelling mass flux was decreasing at 5% per decade, in contrast to an increase of around 2% per decade projected by models (Butchart *et al.*, 2006, 2010; Garcia and Randel, 2008; Li *et al.*, 2008; McLandress and Shepherd, 2009). Although this weakening of the Brewer–Dobson circulation inferred from ERA-Interim is consistent with the observational study of Engel *et al.* (2009) using age of air estimates, there is uncertainty over the reliability of the calculated decrease in upwelling due to its inconsistency (assuming an adiabatic temperature response to changes in upwelling) with the ERA-Interim temperature trends in the tropical lower stratosphere. Using a different diagnostic approach Iwasaki *et al.* (2009) also concluded that the trend estimates were unreliable because of the diversity among the different reanalyses they considered, and because of the short length of the ERA-Interim time series. Therefore, despite the smoother representation of the Brewer–Dobson circulation in ERA-Interim compared to other reanalysis datasets, further development will be required to improve the confidence in the trends estimates.

Acknowledgements

This work was supported by the Joint DECC/Defra Met Office Hadley Centre Climate Programme (GA01101). ECMWF ERA-Interim data used in this study have been provided by ECMWF. The work has benefited from pertinent discussions with Paul Berrisford and Peter Haynes.

References

- Andrews DG, McIntyre ME. 1976. Planetary waves in horizontal and vertical shear: the generalized Eliassen–Palm relation and the mean zonal acceleration. *J. Atmos. Sci.* **33**: 2031–2048.
- Butchart N, Scaife AA. 2001. Removal of chlorofluorocarbons by increased mass exchange between the stratosphere and troposphere in a changing climate. *Nature* **410**: 799–802.
- Butchart N, Scaife A, Bourqui M, de Grandpré J, Hare S, Kettleborough J, Langematz U, Manzini E, Sassi F, Shibata K, Shindell D, Sigmond M. 2006. Simulations of anthropogenic change in the strength of the Brewer–Dobson circulation. *Climate Dyn.* **27**: 727–741.
- Butchart N, Cionni I, Eyring V, Shepherd TG, Waugh DW, Akiyoshi H, Austin J, Brühl C, Chipperfield MP, Cordero E, Dameris M, Deckert R, Dhomse S, Frith SM, Garcia RR, Gettelman A, Giorgetta MA, Kinnison DE, Li F, Mancini E, McLandress C, Pawson S, Pitari G, Plummer DA, Rozanov E, Sassi F, Scinocca JF, Shibata K, Steil B, Tian W. 2010. Chemistry-climate model simulations of 21st century stratospheric climate and circulation changes. *J. Climate* **23**: 5349–5374.
- Butchart N, Charlton-Perez AJ, Cionni I, Hardiman SC, Haynes PH, Krüger K, Kushner PJ, Newman PA, Osprey SM, Perlwitz J, Sigmond M, Wang L, Akiyoshi H, Austin J, Bekki S, Baumgaertner A, Braesicke P, Brühl C, Chipperfield MP, Dameris M, Dhomse S, Eyring V, Garcia RR, Garny H, Jöckel P., Lamarque J-F, Marchand M, Michou M, Morgenstern O, Nakamura T, Pawson S, Plummer DA, Pyle J, Rozanov E, Scinocca JF, Shepherd TG, Shibata K, Smale D, Teyssède H, Tian W, Waugh D, Yamashita Y. 2011. Multi-model climate and variability of the stratosphere. *J. Geophys. Res.* **116**: D05102, DOI: 10.1029/2010JD014995.
- Calvo N, Garcia RR. 2009. Wave forcing of the tropical upwelling in the lower stratosphere under increasing concentrations of greenhouse gases. *J. Atmos. Sci.* **66**: 3184–3196.
- Chun H-Y, Song I-S, Baik J-J, Kim Y-J. 2004. Impact of a convectively forced gravity wave drag parametrization in NCAR CCM3. *J. Climate* **17**: 3530–3547.
- Davies T, Cullen MJP, Malcolm AJ, Mawson MH, Staniforth A, White AA, Wood N. 2005. A new dynamical core for the Met Office's global and regional modelling of the atmosphere. *Q. J. R. Meteorol. Soc.* **131**: 1759–1782.
- Dee DP, Uppala SM, Simmons AJ, Berrisford P, Poli P, Kobayashi S, Andrae U, Balmaseda MA, Balsamo G, Bauer P, Bechtold P, Beljaars ACM, van de Berg L, Bidlot J, Bormann N, Delsol C, Dragani R, Fuentes M, Geer AJ, Haimberger L, Healy SB, Hersbach H, Hólm EV, Isaksen I, Kållberg P, Köhler M, Matricardi M, McNally AP, Monge-Sanz BM, Morcrette J-J, Park B-K, Peubey C, de Rosnay P, Tavolato C, Thépaut J-N, and Vitart F. 2011. The ERA-Interim reanalysis: configuration and performance of the data assimilation system. *Q. J. R. Meteorol. Soc.* **137**: 553–597.
- Dragani R. 2010. 'On the quality of the ERA-Interim ozone reanalyses. Part I: Comparisons with in situ measurements'. ECMWF Technical Report, ERA Report Series (2).
- Dunkerton TJ. 1978. On the mean meridional mass motions of the stratosphere and mesosphere. *J. Atmos. Sci.* **35**: 2325–2333.
- Dunkerton TJ, Hsu C-PF, McIntyre ME. 1981. Some Eulerian and Lagrangian diagnostics for a model stratospheric warming. *J. Atmos. Sci.* **38**: 819–843.
- Eluszkiewicz J, Crisp D, Zurek R, Elson L, Fishbein E, Froidevaux L, Waters J, Grainger RG, Lambert A, Harwood R, Peckham G. 1996. Residual circulation in the stratosphere and lower mesosphere diagnosed from Microwave Limb Sounder data. *J. Atmos. Sci.* **53**: 217–240.
- Engel A, Möbius T, Bönisch H, Schmidt U, Heinz R, Levin I, Atlas E, Aoki S, Nakazawa T, Sugawara S, Moore F, Hurst D, Elkins J, Schauffler S, Andrews A, Boering K. 2009. Age of stratospheric air unchanged within uncertainties over the past 30 years. *Nat. Geosci.* **2**: 28–31.
- Garcia RR, Randel WJ. 2008. Acceleration of the Brewer–Dobson circulation due to increases in greenhouse gases. *J. Atmos. Sci.* **65**: 2731–2739.
- Haynes PH, Marks CJ, McIntyre ME, Shepherd TG, Shine KP. 1991. On the 'downward control' of the extratropical diabatic circulations by eddy-induced mean zonal forces. *J. Atmos. Sci.* **33**: 651–678.
- Holton JR. 1990. On the global exchange of mass between the stratosphere and troposphere. *J. Atmos. Sci.* **47**: 392–395.
- Holton JR, Haynes PH, McIntyre ME, Douglass A, Rood R, Pfister L. 1995. Stratosphere–troposphere exchange. *Rev. Geophys.* **33**: 403–439.
- Houghton JT, Meira Filho LG, Callender BA, Harris N, Kattenberg A, Maskell K. 1995. *Report of Working Group I: The Science of Climate Change, with a Summary for Policymakers (SPM)*. Cambridge University Press: Cambridge, UK.
- Hsu H-H, Hoskins BJ. 1989. Tidal fluctuations as seen in ECMWF data. *Q. J. R. Meteorol. Soc.* **115**: 247–264.
- IFS documentation. 2007. 'Cy31r1, Operational implementation 12 September 2006. Part IV: Physical processes'. ECMWF, 2007. <http://www.ecmwf.int/research/ifsdocs/CY31r1/index.html>
- Iwasaki T, Hamada H, Miyazaki K. 2009. Comparisons of Brewer–Dobson circulations diagnosed from reanalysis. *J. Meteorol. Soc. Jpn* **87**: 997–1006.
- Li F, Austin J, Wilson J. 2008. The strength of the Brewer–Dobson circulation in a changing climate: a coupled chemistry-climate model stimulation. *J. Climate* **21**: 40–57.
- McLlandress C, Shepherd TG. 2009. Simulated anthropogenic changes in the Brewer–Dobson circulation, including its extension to high latitudes. *J. Climate* **22**: 1516–1540.
- Onogi K, Tsutsui J, Koide H, Sakamoto M, Kobayashi S, Hatsushika H, Matsumoto T, Yamazaki N, Kamahori H, Takahashi K, Kadokura S, Wada K, Kato K, Oyama R, Ose T, Mannoji N, Taira R. 2007. The JRA-25 reanalysis. *J. Meteorol. Soc. Jpn* **85**: 369–432.
- Plumb RA, Eluszkiewicz J. 1999. The Brewer–Dobson circulation: dynamics of the tropical upwelling. *J. Atmos. Sci.* **56**: 868–890.
- Randel WJ. 1993. Global variations of zonal mean ozone during stratospheric warming events. *J. Atmos. Sci.* **50**: 3308–3321.
- Randel WJ, Garcia R, Wu F. 2008. Dynamical balances and tropical stratospheric upwelling. 2008. *J. Atmos. Sci.* **65**: 3584–3595.
- Rosenlof KH. 1995. Seasonal cycle of the residual mean meridional circulation in the stratosphere. *J. Geophys. Res.* **100**: 5173–5191.
- Scaife AA, Butchart N, Warner CD, Swinbank R. 2002. Impact of a spectral gravity wave parameterization on the stratosphere in the Met Office Unified Model. *J. Atmos. Sci.* **59**: 1473–1489.
- Simmons A, Uppala S, Dee D, Kobayashi S. 2007. ERA-Interim: new ECMWF reanalysis products from 1989 onwards. *ECMWF Newsletter* No. (110): 25–35.

- Swinbank R O'Neill A. 1994. A stratosphere–troposphere data assimilation system. *Mon. Weather Rev.* **122**: 686–702.
- Uppala SM, Kallberg PW, Simmons AJ, Andrae U, Bechtold VD, Fiorino M, Gibson JK, Haseler J, Hernandez A, Kelly GA, Li X, Onogi K, Saarinen S, Sokka N, Allan RP, Andersson E, Arpe K, Balmaseda MA, Beljaars ACM, Van De Berg L, Bidlot J, Bormann N, Caires S, Chevallier F, Dethof A, Dragosavac M, Fisher M, Fuentes M, Hagemann S, Holm E, Hoskins BJ, Isaksen I, Janssen PAEM, Jenne R, McNally AP, Mahfouf JF, Morcrette JJ, Rayner NA, Saunders RW, Simon P, Sterl A, Trenberth KE, Untch A, Vasiljevic D, Viterbo P, Woollen J. 2005. The ERA-40 re-analysis. *Q. J. R. Meteorol. Soc.* **131**: 2961–3012.
- WMO. 2010. *Scientific Assessment of Ozone Depletion 2010*, Section 4.3.2. World Meteorological Organization: Geneva.